International Journal of Heat and Mass Transfer 52 (2009) 3109–3117

Contents lists available at ScienceDirect

International Journal of Heat and Mass Transfer

journal homepage: www.elsevier.com/locate/ijhmt

Heat/mass transfer in rotating impingement/effusion cooling with rib turbulators

Sung Kook Hong, Dong Hyun Lee, Hyung Hee Cho *

Department of Mechanical Engineering, Yonsei University, Seoul 120-749, Republic of Korea

ARTICLE INFO

Article history:
Received 15 February 2008
Received in revised form 15 January 2009
Accepted 15 January 2009
Available online 25 March 2009

Keywords:
Turbine
Impingement/effusion cooling
Rib turbulators
Rotation

ABSTRACT

A detailed measurement of the heat/mass transfer coefficients on the ribbed surfaces for the rotating impingement/effusion cooling system has been conducted. Three different jet orientations (front, leading, and trailing) were investigated at the same rotating speed and impinging jet Reynolds number of 3000. A naphthalene sublimation method was used to obtain local heat/mass transfer coefficients. Regardless of rib turbulators, the leading and trailing orientations lead to totally changed heat/mass transfer distributions due to the jet deflection, while the Sh distributions of the front orientation were similar to those of the stationary case. For leading and trailing orientations, the influence of crossflow, which deflected wall jets, decreased due to the blockage effect of the rib turbulators. Therefore, the wall jets spread more widely and the interaction between adjacent wall jets along spanwise direction became stronger, enhancing the heat/mass transfer compared to that on smooth surface.

1. Introduction

In gas turbine systems, the achievement of high thermal efficiency is strongly related to the increase in turbine inlet temperature, which is accompanied by the excess thermal load in the component of the gas turbine. Therefore, various cooling techniques have been used to protect the main parts of the gas turbine, such as the combustor liner and turbine blade. Recently, enhanced cooling techniques, combined with conventional cooling methods, have been developed; impingement/effusion cooling is one of these cooling schemes. In impingement/effusion cooling, the inner surfaces of hot components are cooled by the impinging jet cooling, and the outer surfaces that are exposed to hot gases are protected by effusion film cooling. Therefore, this technique provides greater cooling compared to other methods.

Some basic studies on impingement/effusion cooling have been performed in the last few decades. Hollworth and Dagan [1] and Hollworth et al. [2] measured the averaged and local heat transfer coefficients of arrays of turbulent air jets impinging on perforated target surfaces and reported that arrays with staggered vents consistently yielded higher heat transfer rates than impinging jets on solid plates. Andrews et al. [3] studied film cooling performance under the effects of a number of holes for the impingement/effusion cooling system. Metzger and Bunker [4] and Huber and Viskanta [5] reported on the local heat transfer distributions on the surface with a film extraction hole. Cho and Rhee [6] and Rhee et al. [7] investigated local heat/mass transfer and flow characteristics of impingement/effusion cooling under a variety of experimental parameters, such as hole-to-plate spacings, Reynolds numbers, and hole arrangements. Rhee et al. [8] examined the crossflow effects on heat transfer in the impinging/effusion cooling system. They reported that low transfer regions are formed locally between the adjacent effusion holes. Ekkad et al. [9] investigated the effect of crossflow orientation and showed that the orientation condition with smaller crossflow produced higher heat transfer distributions.

To enhance the thermal efficiency, the increase in turbine inlet temperature requires more efficient cooling system for the rotating turbine blade as well as the stationary guide vane and the combustor liner. Therefore, the impingement/effusion cooling system can apply to the rotor blade. There were few studies for regarding the rotating impingement/effusion cooling system, but some for the rotating impinging jet. Epstein et al. [10] investigated the heat transfer characteristics of the leading edge of the turbine blade. They found that the rotation reduced the heat transfer and changed the local heat transfer distributions. Mattern and Hennecke [11] reported on the local heat/mass transfer distributions on the curved impinging plate with regard to various parameters, such as hole-to-hole spacing, hole-to-plate spacing, and jet orientation. Parsons and Han [12,13] showed the regional-averaged Nusselt number on the array jet cooling with and without effusion holes that is applied to the midcore of the blade. Hong et al. [14] investigated the heat transfer characteristics of the array jet in the rotating system with the concave surface. Glezer et al. [15] examined the swirling flow using rotation that is focused on the leading edge region of the turbine blade. They showed that the Coriolis force plays an important role in enhancing the internal heat transfer when its direction

* Corresponding author. Tel.: +82 2 2123 2828; fax: +82 2 312 2159.
E-mail address: hhcho@yonsei.ac.kr (H.H. Cho).

0017-9310/$ - see front matter © 2009 Elsevier Ltd. All rights reserved.
doi:10.1016/j.ijheatmasstransfer.2009.01.031

Nomenclature

d	injection and effusion hole diameter
dy	local sublimation depth of naphthalene
D_h	hydraulic diameter of the test duct
D_{naph}	mass diffusion coefficient of naphthalene vapor in air
H	gap distance between the injection hole and target surface
h_m	local mass transfer coefficient, Eq. (1)
$\dot{m}$	local naphthalene mass transfer per unit area and time
Pr	Prandtl number
P_{hole}	pitch of the injection holes at the injection plate
Re_D	Reynolds number based on hole diameter and the average velocity in the hole
Ro	Rotation number, $\Omega D/v_i$
Sc	Schmidt number
Sh	Sherwood number based on the hole diameter, Eq. (2)
U_{Sh}	Uniformity of Sherwood number, $1 - 0.01\sigma$
x, z	distance from the center of an effusion hole
Ω	rotation velocity

Greek symbols

ρ_s	density of solid naphthalene
$\rho_{v,w}$	naphthalene vapor density on the surface
$\rho_{v,\infty}$	naphthalene vapor density of the injected jet
$d\tau$	test duration
σ	standard deviation of total Sh data measured entire test plate

coincides with a tangential velocity vector of swirling flow. Recently, Iacovides et al. [16] measured the vector profile of the impinging jet under an ultimate rotation condition of Ro = 0.18 and presented the Nusselt number on the impinging surface. They reported that very strong rotation led to the disappearance of all secondary peaks and some of the primary peaks in array jets. Heish et al. [17] examined the effects of jet impinging positions on heat transfer from rib-roughened (square and semi-circular) channels with rotational speeds of up to 600 rpm. Significant heat transfer enhancement was found for the rib-roughened channels and within the ranges of operating parameters considered in the study. However, they only suggested the regional-averaged data using the thermal couple technique.

Among the previous studies, Parsons and Han [13] investigated the heat transfer characteristics of an impingement/effusion cooling scheme, presenting the regional-averaged Nusselt number data. Hong and Cho [18] performed the experiment for impingement/effusion cooling and showed that rotation changed the heat transfer characteristics significantly and generated a low heat transfer region near the effusion hole at high H/d. However, they only dealt with a smooth surface without rib turbulators.

It is well known that the installation of rib turbulators is a method of enhancing heat transfer in many cooling systems [19–23]. Therefore, in the present study, the effect of rib turbulators on the heat/mass transfer characteristics was investigated in regard to the rotating impingement/effusion cooling system, and the data on the ribbed surface were compared with those on the smooth surface.

To prevent hot spots and for better thermal design, not only information on the overall heat transfer coefficient, but also its local variation is required. Therefore, we measured detailed heat/mass transfer coefficients on the effusion plate using a naphthalene sublimation method, which eliminates the conduction and radiation errors inherent in heat transfer experiments. The surface boundary condition is analogous to an isothermal surface in a corresponding heat transfer experiment. The flow characteristics can help in understanding the pattern of local heat/mass transfer characteristics on the effusion plate. Therefore, we also conducted a computational simulation using a commercial program (FLUENT) to obtain the flow patterns in the impingement/effusion cooling system.

2. Experimental apparatus and conditions

2.1. Experimental apparatus

A schematic view of the experimental apparatus is shown in Fig. 1. A test duct with the injection and effusion holes was installed on the rotating plate that had a diameter of 1 m. The room air passed into the test duct through the mechanical seal and was then discharged outside. Air was supplied by the inverter-controlled blower (7.5 kW), and the flow rate was measured using an orifice flowmeter. The temperature of the supplied air was kept constant throughout the heat exchanger using a constant-temperature reservoir. The temperature in the test duct was measured by a multimeter on the rotating plate and was transferred wirelessly by a Bluetooth device. The speed of the rotating plate was controlled by an inverter and a tachometer. The mean rotating radius of the test duct was equal to 350 mm.

Fig. 2 shows the schematics of the test duct and hole arrangements. The height and width of the test duct were 30 mm and 50 mm, respectively, and the hydro diameter of the test duct was 37.5 mm. The diameters of the injection and effusion holes were 5 mm (H/d = 6). In the top view (Fig. 2(b)–(d)), the solid and dotted circles indicate the injection holes and the effusion holes, respectively. The injection plate had two rows of eight injection holes (16 holes total), and the effusion plate had one row of eight effusion holes in staggered arrangement with respect to the injection holes. The ratios of hole spacing to hole diameter (P_{hole}/d) were 4.0 and 6.0 for the spanwise and streamwise directions, respectively.

The rib turbulators were installed between the locations of the injection and effusion holes, as shown in Fig. 2(b)–(d), where, in

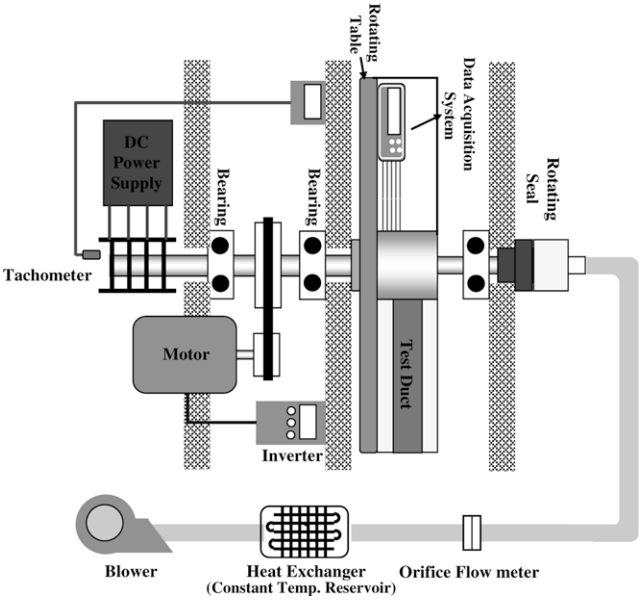

Fig. 1. Schematic view of the experimental facility [18].

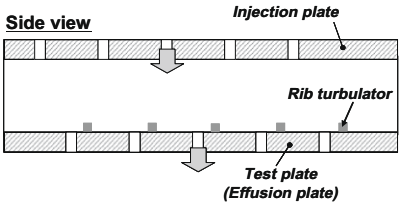

(a) side view

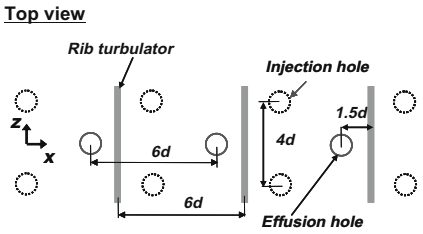

(b) LR-1 position

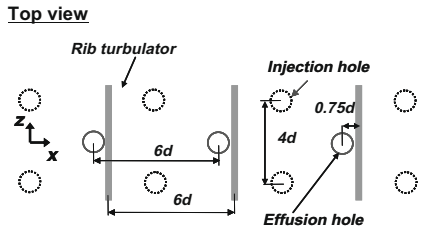

(c) LR-2 position

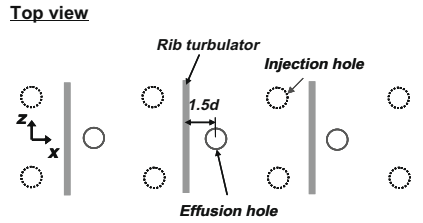

(d) TR position

Fig. 2. Schematic view of the test duct.

each case, rib turbulator position is referred to as LR-1, LR-2, and TR, respectively. For LR-1, the rib was positioned behind the effusion hole by 1.5*d*, and the distance between the rib and effusion hole was 0.75*d* for the LR-2 position. Meanwhile, the rib for TR was positioned in front of the effusion hole by 1.5*d*. It should be noted that the LR-1 position was for the leading orientation, and the TR position was for the trailing orientation, both of which were based on the result of a smooth surface. In all cases, the height and width of each rib turbulator was 1.5 mm, and the length of each rib was equal to the width of the duct.

In the present study, a naphthalene-coated test plate was installed on the test duct to measure the local heat/mass transfer coefficients on the effusion plate. The mass transfer inactive ribs (non-naphthalene coating) are attached to the naphthalene-coated plate which results in distortion of the boundary condition to some extent. However, the active and inactive rib experiment does not make a significant difference in the experimental result as reported by the many groups such as Taslim and Spring [24] and Liou and Hwang [25]. Meanwhile, the details of naphthalene sublimation technique used in the current study are referred to references [6,26].

2.2. Operating conditions

The rotation tests were carried out at a rotating speed of 560 rpm, where the Ro number was 0.032. The jet Reynolds number, based on the injection hole diameter, was set to 3000. The hole-to-plate spacing (H/d) was fixed at 6.0.

Three orientation cases were considered to investigate the effect of jet orientation, as shown in Fig. 3. With respect to the orientation of the jet relative to the axis of rotation, the Coriolis force affected the main impinging jet differentially. When the impinging jet was parallel to the axis of rotation (0°), there was no direct Coriolis force acting on the main impinging jet. However, with an orthogonal orientation to the axis of rotation, the Coriolis force acted on the main impinging jet outward at 90° and inward at −90°. In the present study, the orientations of 0°, 90°, and −90° are referred to as the front, leading, and trailing orientation, respectively.

2.3. Heat/mass transfer coefficient

Using a naphthalene sublimation method, the local mass transfer coefficient is defined as:

$$h_m = \frac{\dot{m}}{\rho_{v,w} - \rho_{v,\infty}} = \frac{\rho_s (dy/d\tau)}{\rho_{v,w}} \tag{1}$$

Since the incoming flow contained no naphthalene, $\rho_{v,\infty}$ is zero. The naphthalene vapor density, $\rho_{v,w}$, was calculated from the perfect gas law, and the naphthalene vapor pressure was obtained from a correlation of Ambrose et al. [27]. The Sherwood number can be expressed as:

$$Sh = h_m d / D_{naph} \tag{2}$$

D_{naph} is the diffusion coefficient of naphthalene vapor in air and the properties of naphthalene, as suggested by Goldstein and Cho [26], were used in this study. The mass transfer coefficients can be converted to the heat transfer coefficients by using the heat and mass transfer analogy by Eckert [28]. The Prandtl number is 0.71 for air, and the Schmidt number is 2.28 for the naphthalene vapor in air at 25 °C. The experiments were conducted at room temperature, and the Lewis number (Pr/Sc) for this study was about 0.31.

$$\mathrm{Nu}/\mathrm{Sh} = (\mathrm{Pr}/\mathrm{Sc})^{0.4}, \quad \mathrm{Nu} = 0.624\mathrm{Sh} \tag{3}$$

In the present study, the uncertainty of the Sherwood number was within ±8.7% in the entire operating range of the measurement, based on a 95% confidence level. The value was calculated using ASME measurement uncertainty methodology, as reported by Abernethy et al. [29].

2.4. Numerical simulation

The numerical simulations were performed using a commercial code, FLUENT (ver. 6.1), to help elucidate the flow characteristics of the rotating impingement/effusion cooling. GAMBIT solid model-

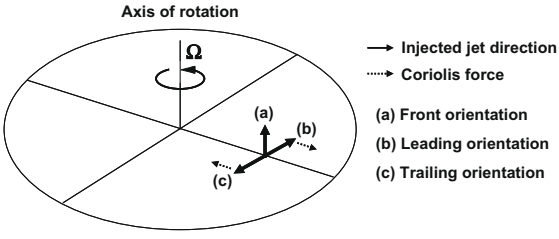

Fig. 3. Schematic view of the orientation of the jet relative to the rotating axis.

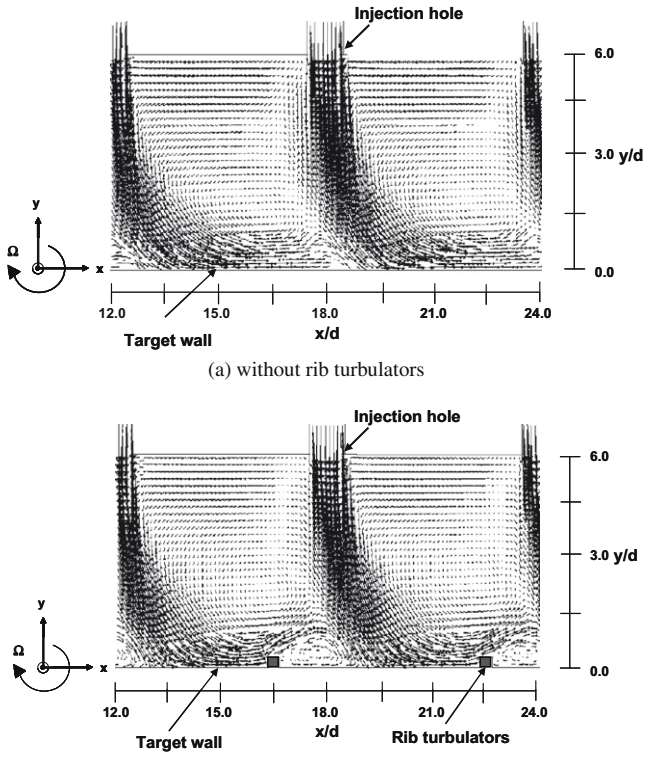

(a) without rib turbulators

(b) with rib turbulators (LR-1 position)

Fig. 4. Velocity vector plot on the injection plane ($z/d = -2.0$) of the leading orientation.

ing created the computation domain, which was modeled by the geometry used in the experimental study. The steady solutions for the turbulent flow field were calculated using a RNG k–ε model with a standard wall function. Different grids were tested to verify the grid independence of the solution, and the results for the grid with 600,000 cells were demonstrated in this study. The convergence of residuals for continuity, momentum, k, and ε were resolved to levels of 10^{-3}.

3. Results and discussion

3.1. Flow characteristics

For the stationary condition, the jet flow was injected normally on the target plate, and the wall jet flow developed axi-symmetrically into the neighboring area and interacted with adjacent wall jets, as reported by Cho and Rhee [6]. However, these injected jet flows were changed significantly by rotation. Fig. 4 shows the relative velocity vector plots on the center plane of injection hole ($z/d = -2.0$) for the rotating condition of the leading orientation. On the smooth surface (Fig. 4(a)), the jet started to deflect toward the outward direction where the Coriolis force acted on that direction in the leading orientation (Fig. 3). Therefore, the injected jet moved outward and then impinged at the position that was approximately 1.0d from the center of the projected injection hole. Most of the jet flow was swept into the deflected direction; then, it collided with the adjacent jet, providing a crossflow-like effect on the injected jet in the downstream region. Fig. 4(b) shows the velocity vectors of the leading orientation with rib turbulators (LR-1 position). The deflected jet flow behavior was similar to that of the case without rib turbulators. However, some discrepancies were observed in the flow near the target wall. The deflected wall jet generated in the upstream region was disturbed by the rib turbulators and formed an upward flow. Therefore, a large recirculating flow was formed behind the rib turbulators, and the crossflow effect on the jet in the downstream region decreased.

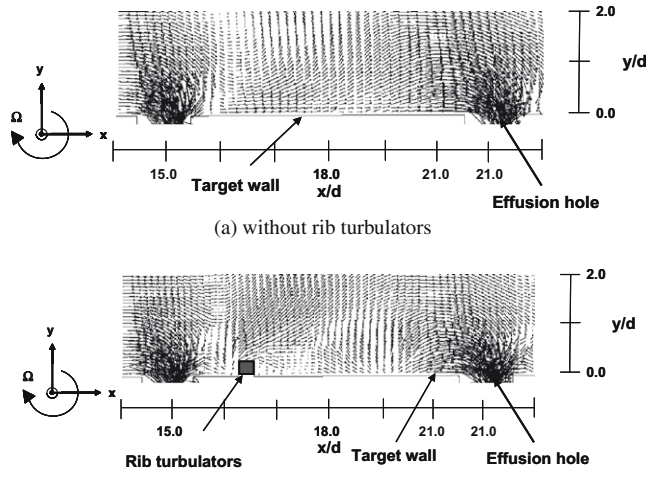

(a) without rib turbulators

(b) with rib turbulators (LR-1 position)

Fig. 6. Velocity vector plot on the effusion plane ($z/d = 0.0$) of the leading orientation.

Fig. 5 shows the relative velocity vectors near the bottom of the plate ($y/d = 0.1$). For both cases, the stagnation point was formed downstream from the center of the projected injection hole due to the rotation effect. However, in the case without the rib turbu-

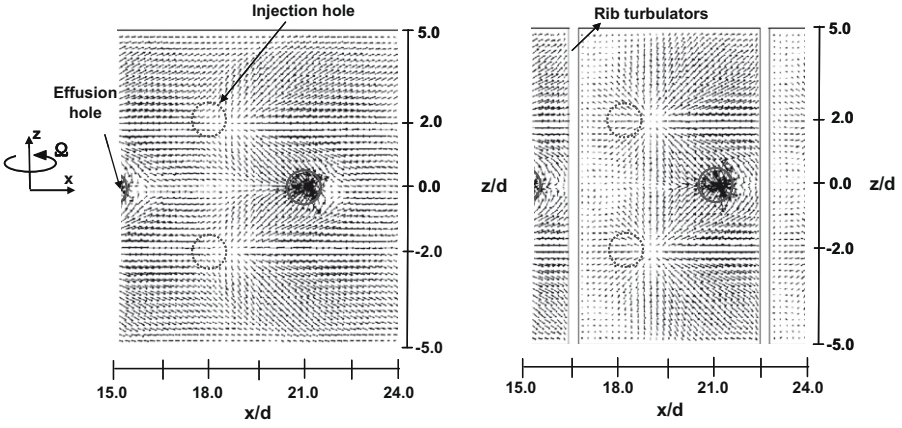

(a) without rib turbulators

(b) with rib turbulators (LR-1 position)

Fig. 5. Velocity vector plot on the bottom plane ($y/d = 0.1$) of the leading orientation.

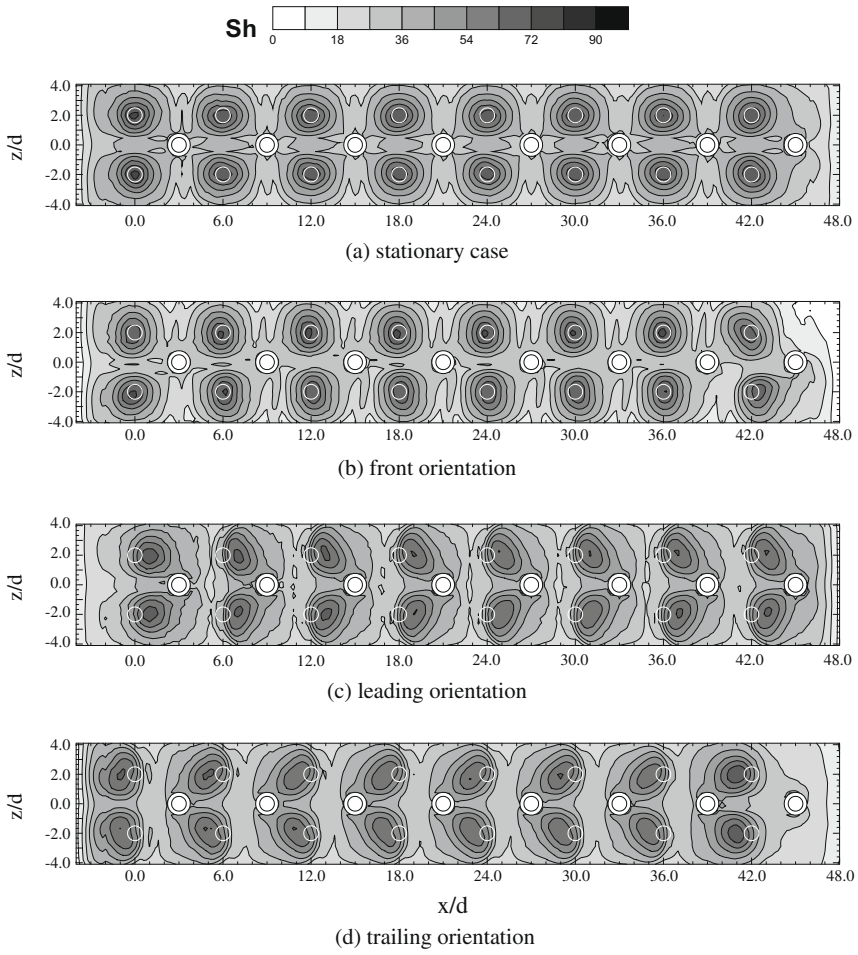

Fig. 7. Contour plots of Sh on the smooth surface for various rotating cases with the impingement/effusion cooling [18].

lators (Fig. 5(a)), the developing flow from the stagnation point was evidently affected by the deflected wall jet, which was generated in the upstream region (crossflow effect). Therefore, the wall jet only spread toward the downstream region, and the interaction between adjacent wall jets was weak at the midway region of $z/d = 0.0$. When the rib turbulators were installed (Fig. 5(b)), the crossflow effect caused by the deflected wall jet decreased near the wall due to the blockage effect of the rib turbulators. Compared to the case without the rib turbulators, the wall jets spread more widely, and the interaction between the wall jets at $z/d = 0.0$ was more excited. This interaction between the wall jets was confirmed at the plane of $z/d = 0.0$, as shown in Fig. 6. The case without the rib turbulators (Fig. 6(a)) showed the typical flow feature caused by the crossflow effect; the near-wall flow moved downstream, and a weak upward flow was formed in the upstream region of effusion hole due to weak interaction of the wall jets, which were drawn into the effusion holes. However, as shown in Fig. 6(b), a strong upward flow was generated around the region of $x/d = 19.0$, which corresponded to the position of the actual stagnation point. It can be inferred from this flow pattern that the interaction between adjacent wall jets occurred strongly, and consequently, the flow mixing was enhanced by the generation of vortices, as reported by Cho and Rhee [6]. Meanwhile, flow acceleration into the effusion hole was observed for both cases because the discharged flow effect was dominant near the effusion hole.

3.2. Heat/mass transfer characteristics

To help understand the basic heat/mass transfer characteristics of rotation, Fig. 7 shows Sh distributions on the smooth surface for the impingement/effusion cooling, as reported by Hong and Cho [18]. In the contour plots, the white and dark circles indicate the projected position of the injection hole and the effusion hole with the aluminum rim, respectively.

For the stationary case (Fig. 7(a)), the Sh distributions appeared periodically as a monotonic decrease from the stagnation point because $H/d = 6$, and the spent air was discharged immediately into the neighboring effusion hole. The Sh distribution of the front orientation (Fig. 7(b)) was similar to that of the stationary case because the influence of the impinging jet was dominant, and the jet flow was only slightly affected by the Coriolis force.

For the leading orientation (Fig. 7(c)), the stagnation region was shifted downstream by $1d$. Moreover, a low heat/mass transfer area was generated behind the effusion hole. This occurred because most of wall jet was deflected into the downstream region, and the wall jet did not cover the upstream region, which was similar to the case of jet injection into the crossflow [8]. As shown in Fig. 7(d), the trailing orientation presented a reverse Sh pattern compared to the leading orientation because the Coriolis force acted in the inward direction instead of the outward direction, as occurred with the leading orientation.

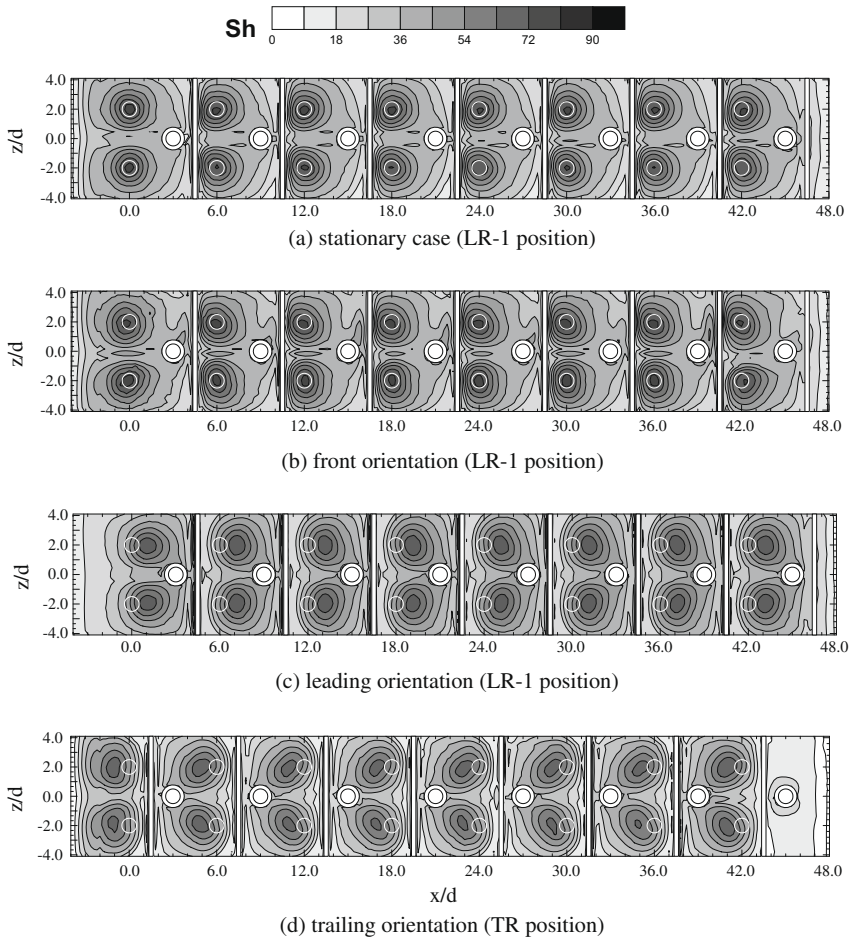

Fig. 8. Contour plots of Sh on the ribbed surface for various rotating cases with the impingement/effusion cooling.

Fig. 8 shows Sh distributions on the ribbed surface for the impingement/effusion cooling, as observed in various rotating cases. In the contour plots, white long rectangles indicate the rib turbulators on the effusion surface. As mentioned, the rib turbulators were installed between the effusion hole and the injection holes, where a low heat/mass transfer region appeared. It was noted that the rib turbulators were in the LR-1 position, except for the trailing orientation, which was in the TR position.

The stationary case presented an asymmetric Sh pattern due to the installation of rib turbulators, as shown in Fig. 8(a). This pattern occurred because the rib turbulators prevented the wall jet from flowing in the upstream direction and isolated the flow within each cell region. Therefore, most of the wall jet leaned downstream and was discharged into the effusion hole in the downstream region. In the front orientation, as shown in Fig. 8(b), the overall heat/mass transfer distributions were similar to those of the stationary case. However, a slightly high Sh region was observed in the upper region of the effusion hole ($z/d \cong 1.0$). This was possibly because the flow developing from the stagnation point rotated in a clockwise direction in the confined area between the rib turbulators with the counterclockwise rotating duct. Thus, a greater amount of wall jet flow was discharged through the upper region of the effusion hole compared to the lower region, producing the discrepancy in Sh distribution near the effusion hole. Fig. 8(c) shows the contour plot of Sh for the leading orientation. The high Sh region enlarged compared to the case without rib turbulators (Fig. 7(c)). This was because the rib turbulators helped the wall jet to spread well into the upstream region of the stagnation point. For the same reason, this feature was also observed for the trailing orientation with opposite Sh distributions, as shown in Fig. 8(d). Therefore, the heat/mass transfer can be enhanced and the low heat/mass transfer region can be reduced by properly positioned rib turbulators in the rotating impingement/effusion cooling system.

Fig. 9 shows the local Sh distributions along $z/d = -2.0$ and 0.0 for the stationary condition. As shown in the contour plots, the heat/mass transfer distributions are quite periodic. Therefore, the data are presented in the range of $10.0 \leqslant x/d \leqslant 30.0$ to clearly observe the effects of the rib turbulators on the local heat/mass transfer. In the local plots, a value of zero represents the position of the effusion holes and rib turbulators.

Along the line at $z/d = -2.0$, the Sh distributions showed the same values in the stagnation region, regardless of the installment of rib turbulators, as shown in Fig. 9(a). However, the rib turbulators lead to a slightly increased Sh in the downstream region ($x/d \cong 14, 20, 26$) of the stagnation point compared to the case without rib turbulators. Meanwhile, near the rib turbulators, the heat/mass transfer rate decreased significantly because the rib turbulators blocked the development of the wall jet toward the upstream region. However, in an actual case, the active rib turbulators will enhance heat transfer in a region with an enlarged surface area and conduction.

In this plot, in which the experimental data from Kooperman [30] were compared in the region of $16.0 \leqslant x/d \leqslant 20.0$, there was a favorable agreement. Some discrepancy was caused by a different Reynolds number, H/d, and s/d.

Along the line at $z/d = 0.0$, as shown in Fig. 9(b), the Sh distributions were changed behind the effusion hole. The higher heat/mass transfer occurred around the effusion hole compared to the case

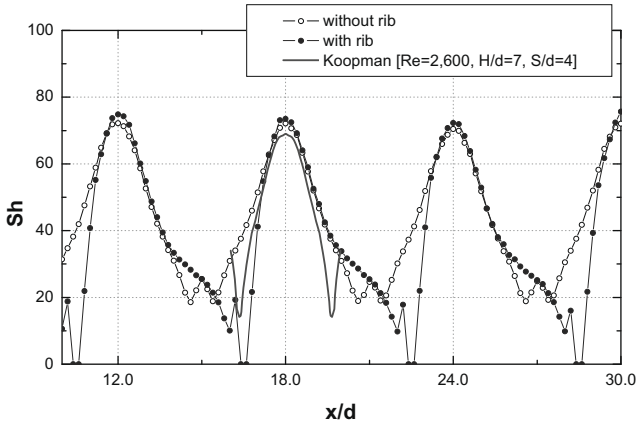

(a) $z/d = -2.0$

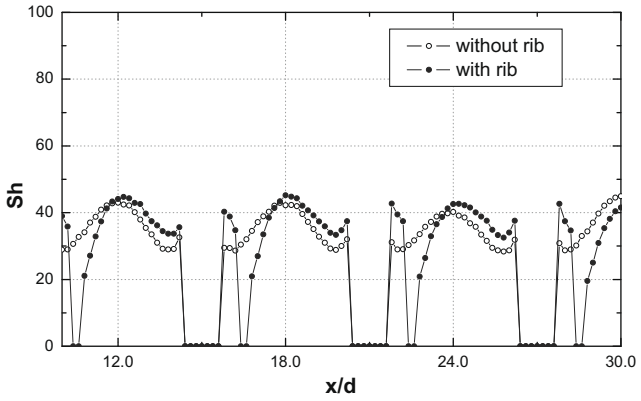

(b) $z/d = 0.0$

Fig. 9. Local plots of Sh on the ribbed surface for the stationary cases with the impingement/effusion cooling.

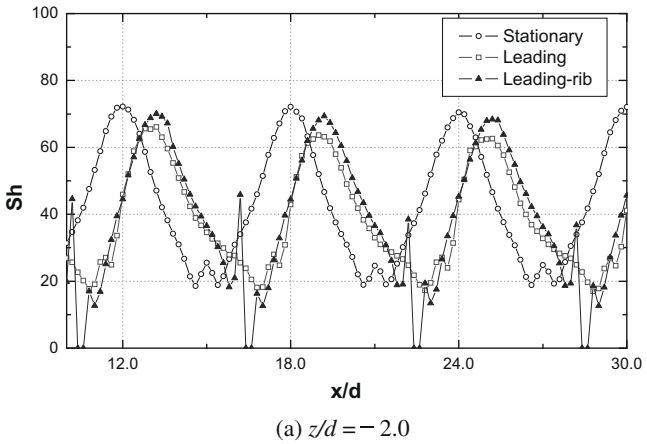

(a) $z/d = -2.0$

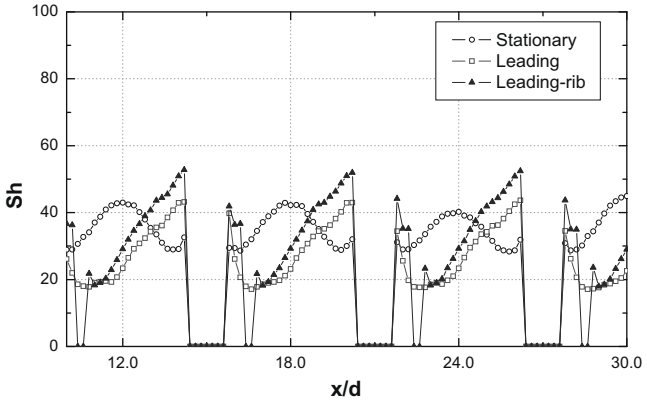

(b) $z/d = 0.0$

Fig. 10. Local plots of Sh on the ribbed surface for the leading orientation with the impingement/effusion cooling.

without rib turbulators. This is because the corner vortex caused by the rib turbulators enhanced the turbulence intensity of the accelerated effusion flow around the effusion hole. Behind x/d = 12, 18, and 24, Sh was slightly higher than that of the case without rib turbulators because the developing wall jet leaned toward the downstream region, and the wall jet interaction along the line at z/d=0.0 became strong. The lower Sh values appeared behind the rib turbulators due to the generation of recirculation flow.

Fig. 10 presents the local Sh distributions for the leading orientation, including the stationary case without rib turbulators. Along the line at $z/d = -2.0$, the stagnation peaks of the rotating cases were shifted toward the downstream side by ld due to jet deflection. The leading orientation without rib turbulators showed a lower peak value than the stationary case. This may be the result of two things: the impingement of jet flow with a decreased momentum caused by jet deflection and the deflected wall jet in the upstream region that affected the injected jet in the downstream region. This phenomenon is similar to the crossflow effect reported by Rhee et al. [8] and Ekkad et al. [9]. However, the rib turbulators protected the injected jet near the bottom surface from the deflected wall jet flow, which was generated in the upstream region. As a result, the leading orientation with rib turbulators yielded a higher peak value than that of the case without rib turbulators. The additional peak was observed just in the front of the rib turbulators due to the generation of a corner vortex.

Along the line at $z/d = 0.0$, as shown in Fig. 10(b), the deflected Sh distributions were formed in the leading orientation, regardless of the presence of rib turbulators. When the rib turbulators were installed, the Sh value was approximately 20% as high as that of the case without rib turbulators. This was caused by the strong interaction between the adjacent wall jets and the generation of a corner vortex in the front of the rib turbulators.

3.3. Effect of rib position

The experiments on different rib turbulator positions have been conducted to investigate the effect of rib turbulator position. Fig. 11 shows the contour plot of Sh at the leading orientation with rib turbulators (LR-2), which was shifted by 0.75d with respect to the LR-1 configuration. The rib position with LR-2 was chosen for the reason that the position of flow reattachment caused by the rib turbulator corresponded to the center of the low heat transfer region. However, the expected heat/mass transfer feature afforded by the rib turbulators was not observed, and the overall Sh distributions were similar to those of the rib turbulators with the LR-1 position (Fig. 8(c)). This implies that the effect of flow reattachment and flow mixing by the rib turbulators is not significant compared to the blockage effect against the deflected wall jet near the wall.

Fig. 12 compares the local Sh value as it relates to the position of rib turbulators. Along the line at $z/d = -2.0$, the level of stagnation peak was the same as that of the LR-1 position due to the blockage effect against the deflected wall jet. The local heat/mass transfer rate was altered slightly by the position of the rib turbulators. The LR-2 position showed a lower Sh value near the rib turbulators than that of the LR-1 position due to enlarged recirculation flow.

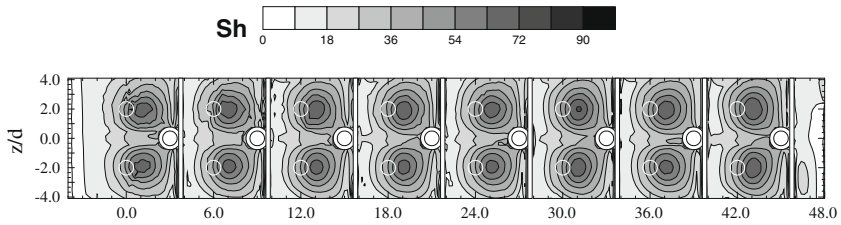

Fig. 11. Contour plot of Sh at LR-2 position for the leading orientation.

Along the line at $z/d = 0.0$, as shown in Fig. 12(b), the impingement by the discharged flow did not occur just behind the effusion hole due to the close rib position relative to the effusion hole, and then the lower Sh region was formed.

In the current study, the change of rib position does not make a significant difference in local heat transfer. However, the installation of ribs produces the rib-induced secondary flow and confinement/protection of wall jet flow from crossflow in the local area. Therefore, the orientation of ribs could be one of important parameters as reported in the previous studies using the various orientations and shapes of ribs [19–21]. Further experiment might be needed to optimize the local heat transfer based on the required operating and geometry condition.

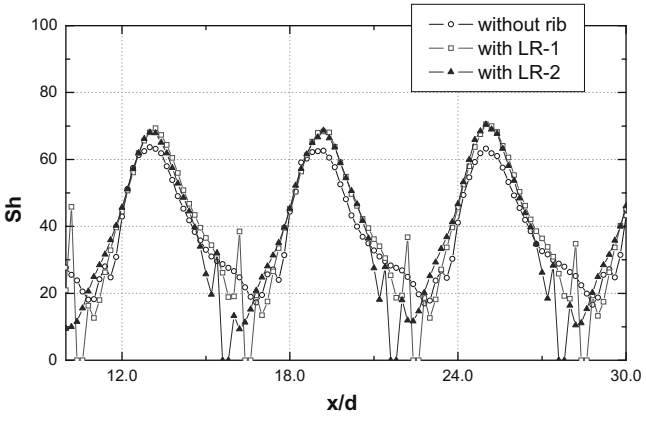

(a) $z/d = -2.0$

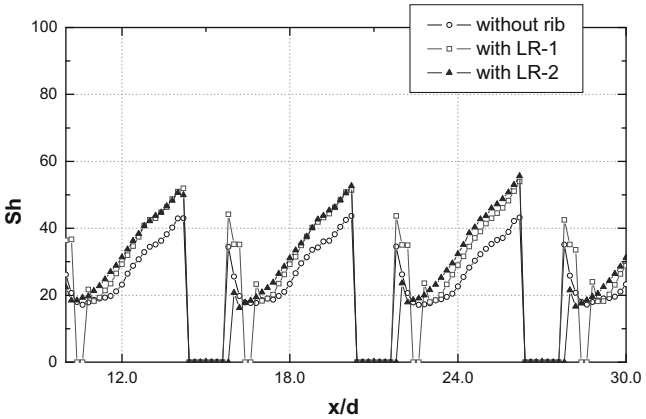

(b) $z/d = 0.0$

Fig. 12. Local plots of Sh at different rib turbulator positions for the leading orientation.

3.4. Averaged heat/mass transfer

Fig. 13 compares the averaged Sh values as they relate to the installation of rib turbulators. It was noted that the averaged values were calculated in the region of $12 \leqslant x/d \leqslant 30$ and $-4.1 \leqslant z/d \leqslant 4.1$, excluding the areas of the effusion hole and the rib turbulators.

There was a slight difference in the averaged Sh values, although the local heat/mass transfer characteristics were changed greatly by rotation. For the leading and trailing orientations, the rib turbulators enhanced the averaged Sh value by approximately 8%. This is mainly because the crossflow effect by the deflected wall jet decreased, as manifested by the local Sh distributions. Meanwhile, the averaged values for the stationary and front cases were similar to that of the case without the rib turbulators. Therefore, the installation of rib turbulators provided a slightly favorable effect for leading and trailing orientations by reducing the wall jet deflection phenomenon.

Fig. 14 shows the Sh uniformity to examine the uniformity of heat/mass transfer rates on the entire test surface. The installation of rib turbulators led to a slight decrease in Sh uniformity. This was because the rib turbulators produced a great deviation in the heat/mass transfer rate: the low Sh region by recirculation flow behind the rib turbulators and the steep Sh increase in front of the rib turbulators. The degradation of Sh uniformity was observed in all tested cases with rib turbulators.

4. Conclusions

This paper investigated the heat/mass transfer characteristics on the ribbed surface for the rotating impingement/effusion cooling and compared the collected data with the results from the

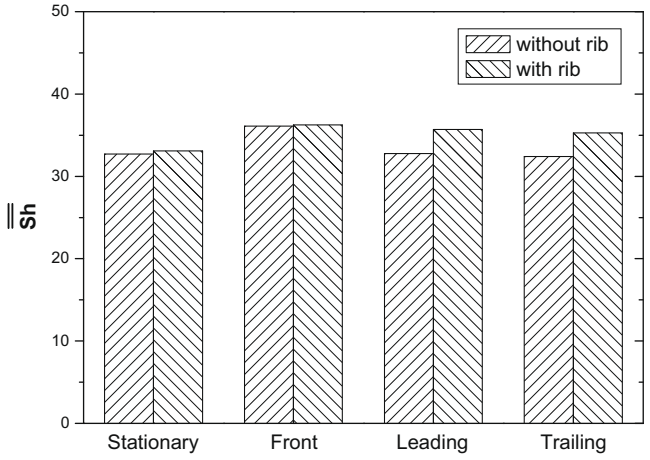

Fig. 13. Averaged Sh value for various rotating cases depending on installation of rib turbulators.

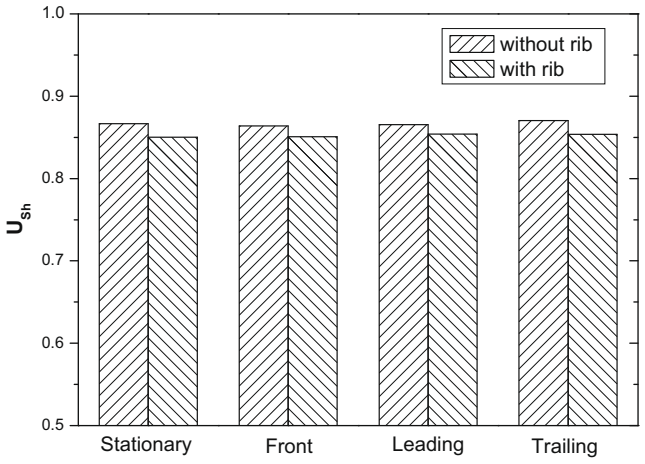

Fig. 14. Sh uniformity for various rotating cases depending on installation of rib turbulators.

studies on the smooth surface. The results are summarized as follows:

1. Regardless of the rib turbulators, the leading and trailing (orthogonal) orientations led to totally changed heat/mass transfer distributions due to the jet deflection phenomenon. For the front (parallel) orientation, the Sh distributions were similar to those of the stationary case.

2. When the rib turbulators were installed at the stationary and front cases, asymmetric Sh distributions were formed because the rib turbulators confined the development of the wall jet in each region between the rib turbulators.

3. For the leading and trailing orientations on the ribbed surface, the crossflow effect caused by the deflected wall jet was reduced due to the blockage effect of the rib turbulators. Therefore, the wall jets spread more widely and the interaction between adjacent wall jets along the spanwise direction became stronger, enhancing the heat/mass transfer compared to the case without rib turbulators. Behind the effusion hole, higher heat/mass transfer was attained because a corner vortex caused by the rib turbulators enhanced the turbulence intensity in the accelerated effusion flow.

4. The change in position of the rib turbulators slightly affected the local heat/mass transfer. This implies that the effect of flow reattachment and flow mixing by the rib turbulators was not significant compared to the blockage effect against the deflected wall jet.

5. For the leading and trailing orientations, the rib turbulators increased the averaged Sh value by approximately 8%. However, the installation of rib turbulators led to a slight decrease in Sh uniformity because the rib turbulators produced a great deviation of the heat/mass transfer rate.

Acknowledgement

This work was supported partially by the Electric Power Industry Technology Evaluation and Planning.

References

[1] B.R. Hollwarth, L. Dagan, Arrays of impinging jets with spent fluid removal through vent holes on the target surface part 1: average heat transfer, J. Eng. Power 102 (1980) 994–999.
[2] B.R. Hollwarth, G. Lehmann, J. Rosiczkowski, Arrays of impinging jets with spent fluid removal through vent holes on the target surface part 2: local heat transfer, J. Eng. Power 105 (1983) 393–402.
[3] G.E. Andrews, A.A. Asere, C.I. Hussain, M.C. Mkpadi, A. Nazari, Impingement/effusion cooling: overall wall heat transfer, ASME 88-GT-290, 1988.
[4] D.E. Metzger, R.S. Bunker, Local heat transfer in internally cooled turbine airfoil leading edge regions: part II-impingement cooling with film coolant extraction, J. Turbomachinery 112 (1990) 459–466.
[5] A.M. Huber, R. Viskanta, Effect of jet–jet spacing on convective heat transfer to confined, impinging, arrays of axisymmetric air jets, Int. J. Heat Mass Transfer 37 (1994) 2859–2869.
[6] H.H. Cho, D.H. Rhee, Local heat/mass transfer measurement on the effusion plate in impingement/effusion cooling system, J. Turbomachinery 123 (2001) 601–608.
[7] D.H. Rhee, J.H. Choi, H.H. Cho, Heat (mass) transfer on effusion plate in impingement/effusion cooling systems, J. Thermophys. Heat Transfer 17 (1) (2003) 95–102.
[8] D.H. Rhee, J.H. Choi, H.H. Cho, Flow and heat (mass) transfer characteristics in an impingement/effusion cooling system with crossflow, J. Turbomachinery 125 (2003) 74–82.
[9] S.V. Ekkad, Y. Huang, J.C. Han, Impingement heat transfer on a target plate with film cooling holes, J. Thermophys. Heat Transfer 13 (4) (1999) 522–528.
[10] A.H. Epstein, J.L. Kerrebrock, J.J. Koo, U.Z. Preiser, Rotational effects on impingement cooling, GTL Report No. 184, 1985.
[11] C. Mattern, D.K. Hennecke, The influence of rotation on impingement cooling, ASME 96-GT-161, 1996.
[12] J.A. Parsons, J.C. Han, Rotation effect on jet impingement heat transfer in smooth rectangular channel with heated target walls and radially outward cross flow, Int. J. Heat Mass Transfer 41 (1998) 2059–2071.
[13] J.A. Parsons, J.C. Han, Rotation effect on jet impingement heat transfer in smooth rectangular channels with heated target walls and film coolant extraction, ASME 96-WA/HT-9, 1996.
[14] S.K. Hong, D.H. Lee, H.H. Cho, Heat/mass transfer measurement on concave surface in rotating jet impingement, J. Mech. Sci. Tech. 22 (2008) 1952–1958.
[15] B. Glezer, H.K. Moon, J.L. Kerrebrock, J. Bons, G. Guenette, Heat transfer in a rotating radial channel with swirling internal flow, ASME 98-GT-214, 1998.
[16] H. Iacovides, D. Kounadis, B.E. Launder, J. Li, Z. Xu, Experimental study of the flow and thermal development of a row of cooling jets impinging on a rotating concave surface, J. Turbomachinery 127 (2005) 222–229.
[17] S.S. Hsieh, H.H. Tsai, S.C. Chan, Local heat transfer in rotating square-rib-roughened and smooth channels with jet impingement, Int. J. Heat Mass Transfer 47 (2004) 2769–2784.
[18] S.K. Hong, H.H. Cho, Effect of rotation on heat/mass transfer for an impingement/effusion cooling system, ASME GT2007-27265, 2007.
[19] K.M. Kim, Y.Y. Kim, D.H. Lee, D.H. Rhee, H.H. Cho, Local heat/mass transfer phenomena in rotating passage part 2: angled ribbed passage, J. Thermophys. Heat Transfer 20 (4) (2006) 199–210.
[20] W.M. Yan, H.C. Liu, C.Y. Soong, W.-J. Yang, Experimental study of impinging heat transfer along rib-roughened walls by using transient liquid crystal technique, Int. J. Heat Mass Transfer 48 (2005) 2420–2428.
[21] W.M. Yan, S.C. Mei, Measurement of detailed heat transfer along rib-roughened surface under arrays of impinging elliptic jets, Int. J. Heat Mass Transfer 49 (2006) 159–170.
[22] C. Gau, I.C. Lee, Flow and impingement cooling heat transfer along triangular rib-roughened walls, Int. J. Heat Mass Transfer 43 (2000) 4405–4418.
[23] D. Cavellero, G. Tanda, An experimental investigation of forced convection heat transfer in channels with rib turbulators by means of liquid crystal thermography, Exp. Thermal Fluid Sci. 26 (2002) 115–121.
[24] M.E. Taslim, S.D. Spring, Effects of turbulator profile and spacing on heat transfer and friction in a channel, J. Thermophys. Heat Transfer 8 (1994) 555–562.
[25] T.M. Liou, J.J. Hwang, Effect of ridge shapes on turbulent heat transfer and friction in a rectangular channel, Int. J. Heat Mass Transfer 36 (1993) 931–940.
[26] R.J. Goldstein, H.H. Cho, A review of mass transfer measurement using naphthalene sublimation, Exp. Thermal Fluid Sci. 10 (1995) 416–434.
[27] D. Ambrose, I.K. Lawrenson, C.H.S. Sparke, The vapor pressure of naphthalene, J. Chem. Thermodyn. 7 (1975) 1173–1176.
[28] E.R.G. Eckert, Analogies to heat transfer processes. In: Measurements in Heat Transfer, second ed. Hemisphere, New York, 1986, pp. 397–423.
[29] R.B. Abernethy, R.P. Benedict, R.B. Dowdell, ASME measurement uncertainty, J. Fluid Eng. 107 (1985) 161–164.
[30] R.N. Koopman, E.M. Sparrow, Local and averaged transfer coefficients due to an impinging row of jets, Int. J. Heat Mass Transfer 19 (1975) 673–683.